HEIMDALL: A Modular Framework for Tokenization in Single-Cell Foundation Models

Ellie Haber[1,*], Shahul Alam[2,*], Nicholas Ho[2,*], Renming Liu[2], Evan Trop[1], Shaoheng Liang[2], Muyu Yang[2], Spencer Krieger[2,†], and Jian Ma[2,†]

[1]Machine Learning Department, School of Computer Science,
Carnegie Mellon University, Pittsburgh, PA 15213, USA
[2]Ray and Stephanie Lane Computational Biology Department, School of Computer Science,
Carnegie Mellon University, Pittsburgh, PA 15213, USA
[*]These authors contributed equally.
[†]Correspondence: skrieger@cs.cmu.edu (S.K.) and jianma@cs.cmu.edu (J.M.)

Abstract

Foundation models trained on single-cell RNA-sequencing (scRNA-seq) data have rapidly become powerful tools for single-cell analysis. Their performance, however, depends critically on how cells are tokenized into model inputs – a design space that remains poorly understood. Here, we present HEIMDALL, a comprehensive framework and open-source toolkit for systematically evaluating tokenization strategies in single-cell foundation models (scFMs). HEIMDALL decomposes each scFM into modular components: a gene identity encoder ($F_{\mathbf{G}}$), an expression encoder ($F_{\mathbf{E}}$), and a "cell sentence" constructor ($F_{\mathbf{C}}$) with submodules (ORDER, SEQUENCE, and REDUCE) enabling fine-grained control and attribution. Using a transformer trained from scratch, we evaluate tokenization strategies for cell type classification across challenging transfer learning settings – cross-tissue, cross-species, and spatial gene-panel shifts – and separately assess reverse perturbation prediction. Tokenization choices show minimal impact in-distribution but are decisive under distribution shift, with $F_{\mathbf{G}}$ and ORDER driving the largest gains and $F_{\mathbf{E}}$ providing additional improvements. HEIMDALL further shows how existing strategies can be recombined to enhance generalization. By standardizing evaluation and providing an extensive library, HEIMDALL establishes a foundation for reproducible, systematic exploration of single-cell tokenization and accelerates the development of next-generation scFMs.

Introduction

Foundation models are emerging as a central and rapidly expanding focus in machine learning for biology, fueling advances in protein structure prediction [1], genomics [2], and clinical applications [3]. In parallel, single-cell foundation models (scFMs) [4–10], enabled by large-scale single-cell RNA-seq (scRNA-seq) atlases [11–13], have gained increasing attention. These models are pretrained on massive single-cell datasets and finetuned for downstream tasks such as cell type annotation, perturbation prediction, batch integration, and gene regulatory network inference [14]. While conceptually similar, scFMs differ in critical design choices, including the scale and composition of the pretraining corpus, the pretraining objective, and the cell tokenization scheme – referred to hereafter as the "tokenizer" – used to represent a cell's expression profile. Among these, the choice of tokenizer is particularly subjective, as there is no obvious biologically grounded way to tokenize gene identities and expression values. This complicates direct adoption of strategies from natural language processing or computer vision, where data are intrinsically sequential and tokenization is well established [15]. As a result, each scFM introduces its own tokenizer, embedding different biological priors as inductive biases. However, without a unifying framework for evaluating these choices, developing an appropriate tokenizer remains a major challenge.

Previous efforts to evaluate scFMs have compared the performance of large pretrained models under finetuning and zero-shot regimes [14, 16–18]. However, such comparisons offer limited insight into which design decisions actually drive performance differences, as variation in model size, dataset scale, and context length confounds fair evaluation. Consequently, bespoke methods tailored to specific tasks often outperform scFMs [17–19], underscoring the need to better understand the intrinsic capacities and limitations of these models. Recent benchmarks have examined aspects of the scFM lifecycle, including downstream task performance [14, 20], pretraining dataset size [19, 21], and pretraining objectives [14, 22, 23]. Despite these efforts, a central question remains unexplored: which choice of tokenizer best enables scFMs to generalize robustly to unseen data and diverse downstream tasks? As established in other domains, tokenization is central to unlocking the representational capacity of sequence models [24, 25], making this question critical for guiding future scFM development.

To address this gap, we present HEIMDALL, a unifying framework and open-source toolkit for systematic evaluation of tokenizers in scFMs. HEIMDALL introduces a modular decomposition of tokenizers that captures the diversity of existing approaches while enabling the implementation of new strategies. Using this framework, we assess tokenizer performance on carefully designed downstream tasks testing generalization across genes, technologies, and tissues. We show that hybrid tokenizers combining elements from existing scFMs can outperform individual strategies. By standardizing evaluation and enabling reproducibility, HEIMDALL provides a foundation for advancing state-of-the-art approaches in transfer learning for single-cell genomics. Moreover, as an open-source resource, HEIMDALL empowers the community to contribute new tokenizers, extend benchmarks, and collectively establish the design principles that will guide the next generation of scFMs.

Results

Overview of HEIMDALL

In the HEIMDALL paradigm, the tokenizer maps a high-dimensional gene expression vector to a sequence of "tokens" as input for a sequence-based model such as a transformer. We abstract the functionality of tokenizers into three functional modules: $F_{\mathbf{G}}$, $F_{\mathbf{E}}$ and $F_{\mathbf{C}}$ (**Fig.** 1A). The gene embedding module $F_{\mathbf{G}}$ encodes the *identity* of a gene by incorporating prior biological knowledge; the expression embedding module $F_{\mathbf{E}}$ encodes the expression *value* of a gene by incorporating cell- or dataset-level statistics; and the aggregation module $F_{\mathbf{C}}$ integrates $F_{\mathbf{G}}$ and $F_{\mathbf{E}}$ outputs to assemble the final sequence-based representation of a cell. This formulation, which aggregates gene-level representations into a cell-level embedding, aligns with the standard formulation for universal representations of virtual cells [26]. For additional modularity, $F_{\mathbf{C}}$ is subdivided into ORDER, SEQUENCE and REDUCE components (**Fig.** S1): ORDER defines the intrinsic ordering of gene tokens, SEQUENCE selects which genes to include and constructs the token sequence, and REDUCE combines gene and expression encodings into a unified representation. Together, this modularization abstracts and generalizes key tokenization design decisions in the scFM literature. Additional details of the tokenizer abstraction can be found in **Methods**.

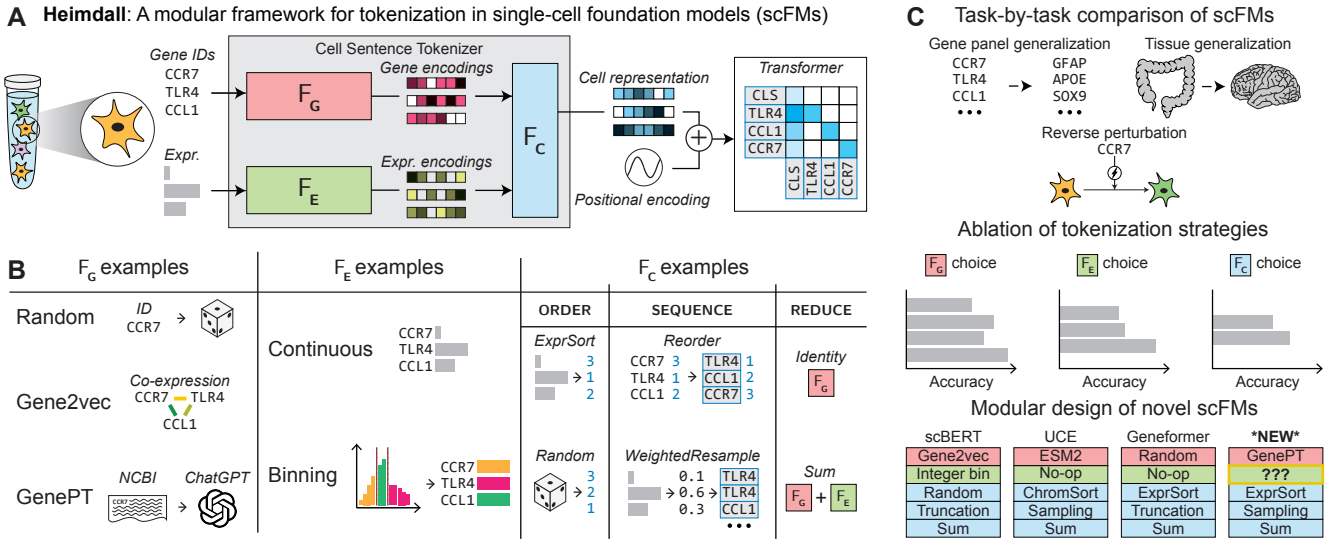

Figure 1: Overview of the HEIMDALL framework for single-cell foundation models (scFMs). A. Modular conceptualization of scFMs in HEIMDALL. Gene identities and expression values from each single-cell input are processed by a cell tokenization scheme (tokenizer) that generates a sequence-based "cell sentence". The tokenizer is decomposed into three modules: a gene identity encoder ($F_{\mathbf{G}}$), an expression encoder ($F_{\mathbf{E}}$), and a cell constructor ($F_{\mathbf{C}}$). The tokenizer output is then passed to a sequence-based model (e.g., a transformer). **B.** Example implementations of the modular components, drawn from prior scFM literature. **C.** Applications of HEIMDALL for systematic design and evaluation of scFMs.

This interface enables HEIMDALL to reproduce input cell representation strategies from existing models. Using this abstraction, we reimplemented tokenizers from five top scFMs – scGPT [4], Geneformer [5], scFoundation [8], scBERT [9], and UCE [10] – denoted with a -tok suffix (e.g., Geneformer-tok) to distinguish them from their pretrained counterparts. These reimplementations yield concrete

modular implementations of $F_{\mathbf{G}}$, $F_{\mathbf{E}}$ and $F_{\mathbf{C}}$ (**Fig.** 1B), with a comprehensive mapping of representative scFMs onto the HEIMDALL tokenizer decomposition summarized in **Table** S1.

The decoupling of tokenization from the sequence model and downstream tasks in HEIMDALL enables fair and measured comparisons of scFMs (**Fig.** 1C, top). By using a fixed set of hyperparameters for model training, HEIMDALL can control the effects of model and dataset size, model architecture, context length, positional encoding, and other elements. It also enables precise ablations of top-performing scFMs (**Fig.** 1C, middle) by swapping concrete implementations of tokenizer modules provided by HEIMDALL with the defaults used by the scFM. To attribute performance differences specifically to tokenization and enable scalable experiments, we forego pretraining and instead train all models from scratch. This allows us to compare tokenizers in a compute-efficient manner without making claims as to the pretraining objectives of existing scFMs. Beyond reproducing and dissecting existing scFMs, HEIMDALL facilitates modular design of novel tokenizers (**Fig.** 1C, bottom). Novel tokenizers can be constructed by mixing and matching HEIMDALL's module implementations, while new modules can be seamlessly integrated into the framework.

We demonstrate HEIMDALL's capabilities using three challenging single-cell transfer-learning benchmarks – tissue shift (training on one organ, testing on another), cross species shift (training on species, testing on another), and gene-panel shift (predicting with unseen or sparsely overlapping genes). We further evaluate a paired-cell reverse perturbation prediction task, where the model infers a perturbation from a target cell state. Fundamentally, scFMs can only become useful and outperform bespoke methods once they learn robust, generalizable representations of cells. We consider these four downstream prediction tasks as interpretable, easy-to-optimize benchmarks that probe the cellular representations output by tokenizers to meaningfully capture and represent cellular identity.

Together, our development and applications highlight HEIMDALL's potential to serve as a foundation for the rigorous, systematic, and measured development of high-performing scFMs.

Evaluating the cross-tissue generalization capacity of scFMs

To evaluate how effectively different tokenizers support transfer learning across biological contexts, we constructed a cell type classification benchmark that measures cross-tissue generalization using a subset of the scTab CELLxGENE census [27] (referred to as the `sc-tab` dataset; see **Methods** for details). Models were trained on cells from the colon and small intestine and evaluated on cells from the brain across 15 shared cell types, providing a direct test of cross-tissue generalization (**Fig.** 2A).

We benchmarked tokenizers using matched conditions, including model size, context length, and no pretraining. We observed minimal performance variation across tokenizers, with Geneformer-tok performing best with a Matthews correlation coefficient (MCC) of 0.40, scBERT-tok and scFoundation-tok performing similarly (0.39), scGPT-tok slightly lower (0.38), and UCE-tok lowest (0.36). These differences were within run-to-run variability (s.d. 0.01-0.02) and overlapped with a linear baseline using raw gene expression (0.40), indicating that tokenizer choice has limited in-distribution impact for this task. Qualitative assessments using UMAP visualizations and confusion matrices corroborated this ranking (**Fig.** 2D-E).

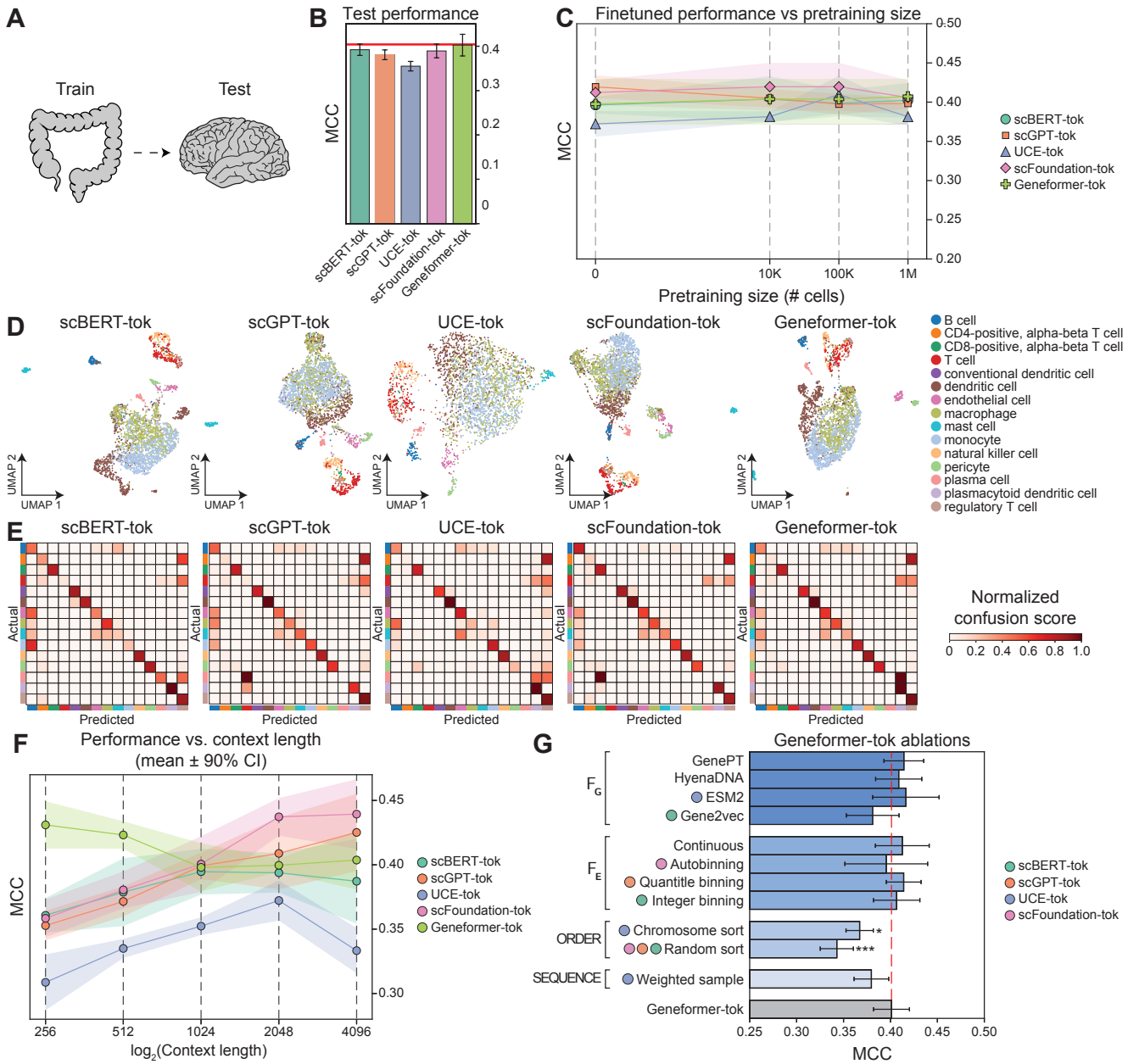

Figure 2: Comparison of scFM generalization performance on held-out tissue contexts using HEIMDALL. **A.** Schematic of the cross-tissue generalization task, where models are trained on colon and intestine cells and evaluated on brain cells. **B.** Performance (MCC; mean $\pm$ s.d. across $n = 10$ random seeds) of five scFMs tokenizers – scBERT-tok, scGPT-tok, UCE-tok, scFoundation-tok, and Geneformer-tok) – on the held-out brain dataset. **C.** Effect of pretraining scale: performance of tokenizers pretrained on progressively larger corpora and fine-tuned on `sc-tab` (x-axis: pretraining corpus size; 0 = no pretraining with random initialization). Error bars show s.d. across $n = 5$ random seeds. **D.** UMAP visualizations of the best-performing run for tokenization strategy, colored by ground-truth labels on the held-out brain dataset. **E.** Row-normalized confusion matrices of predicted versus true labels for each tokenizer. **F.** Performance across context lengths (256-4096 tokens; x-axis in log scale); error bars show s.d. across $n = 5$ random seeds. **G.** Module ablation of the best-performing tokenizer, Geneformer-tok, across HEIMDALL modules ($F_{\mathbf{G}}$, $F_{\mathbf{E}}$, ORDER, SEQUENCE); error bars show s.d. across $n = 6$ random seeds. Significance was assessed using paired tests with Holm correction (p < 0.05, p < 0.01, p < 0.001).

To determine whether these conclusions extend to pretrained scFMs, we compared models trained from scratch to those pretrained on 10k, 100k, and 1M cells using a masked language modeling (MLM) objective and then finetuned (**Fig.** 2C). Across tokenizers, we observed limited benefit from MLM pretraining. scFoundation-tok showed small, monotonic gains with additional pretraining (± 0.01), Geneformer-tok and scBERT-tok changed minimally, scGPT-tok declined modestly with larger pretraining sets, and UCE-tok improved modestly ($+0.03$). These results indicate that tokenizer choice – rather than pretraining – is the primary determinant of cross-tissue performance in this setting, with pretraining exerting only a marginal effect.

We next assessed how context length (tokens per cell) influences tokenizer performance in cross-tissue generalization (**Fig.** 2F). Performance increased with context length up to 2,048 tokens for scGPT-tok, scBERT-tok, and scFoundation-tok, after which it plateaued. This plateau can be attributed to the typical number of expressed genes per cell in `sc-tab`, with a median of 1,006 and an interquartile range of 598-1,637. Beyond 2,048 tokens, additional capacity primarily captures unexpressed or padded tokens, contributing limited new signal. Tokenization strategies that explicitly rank or resample genes exhibited distinctive scaling behavior: Geneformer-tok performance declined between 256 and 1,024 tokens before plateauing, whereas UCE-tok became unstable beyond 2,048 tokens.

To identify which tokenizer components drive cross-tissue generalization, we ablated the Geneformer-tok configuration within `sc-tab` using HEIMDALL (**Fig.** 2G). As all current tokenizers share the same REDUCE function, we varied the remaining modules ($F_{\mathbf{G}}$, $F_{\mathbf{E}}$, ORDER, and SEQUENCE). Beyond the modules used in existing scFM tokenizers, we introduced three new variants: GenePT-based [6] and HyenaDNA-based gene identity embeddings for $F_{\mathbf{G}}$, and a continuous expression encoding for $F_{\mathbf{E}}$ (see **Methods**). Changes to $F_{\mathbf{G}}$ had limited effect: ESM2 (0.42 ± 0.03) and GenePT (0.41 ± 0.02) performed within the variability of the Geneformer-tok baseline with random embeddings (0.40 ± 0.02), indicating no meaningful $F_{\mathbf{G}}$-dependent differences for this task. Adding explicit expression encodings in $F_{\mathbf{E}}$ likewise did not yield consistent gains; scGPT-tok's quantile binning matched the default No-Op $F_{\mathbf{E}}$ (0.41 ± 0.02 versus 0.40 ± 0.02). Within the ORDER module, Geneformer-tok's expression-based ORDER remained best, showing significant gains over chromosome order (Holm-adjusted $p < 0.05$) and random order ($p < 0.01$) in paired tests across seeds; modifications to SEQUENCE did not surpass the default truncation-to-context strategy.

Overall, these ablations suggest that Geneformer-tok's current formulation is already well specified for cross-tissue generalization, with limited room for further improvement via tokenization alone. Its advantage appears to arise primarily from the expression-sorting ORDER, which implicitly injects expression information into the cell tokenization despite the absence of an explicit $F_{\mathbf{E}}$. Together, these results demonstrate how HEIMDALL facilitates systematic dissection of existing tokenizers and guides principled improvements.

Evaluating the cross-species generalization capacity of scFMs

The transcriptional programs, regulatory modules, and signaling pathways that define cell identity are highly conserved across mammals [28]. However most scFMs are pretrained on a single species and

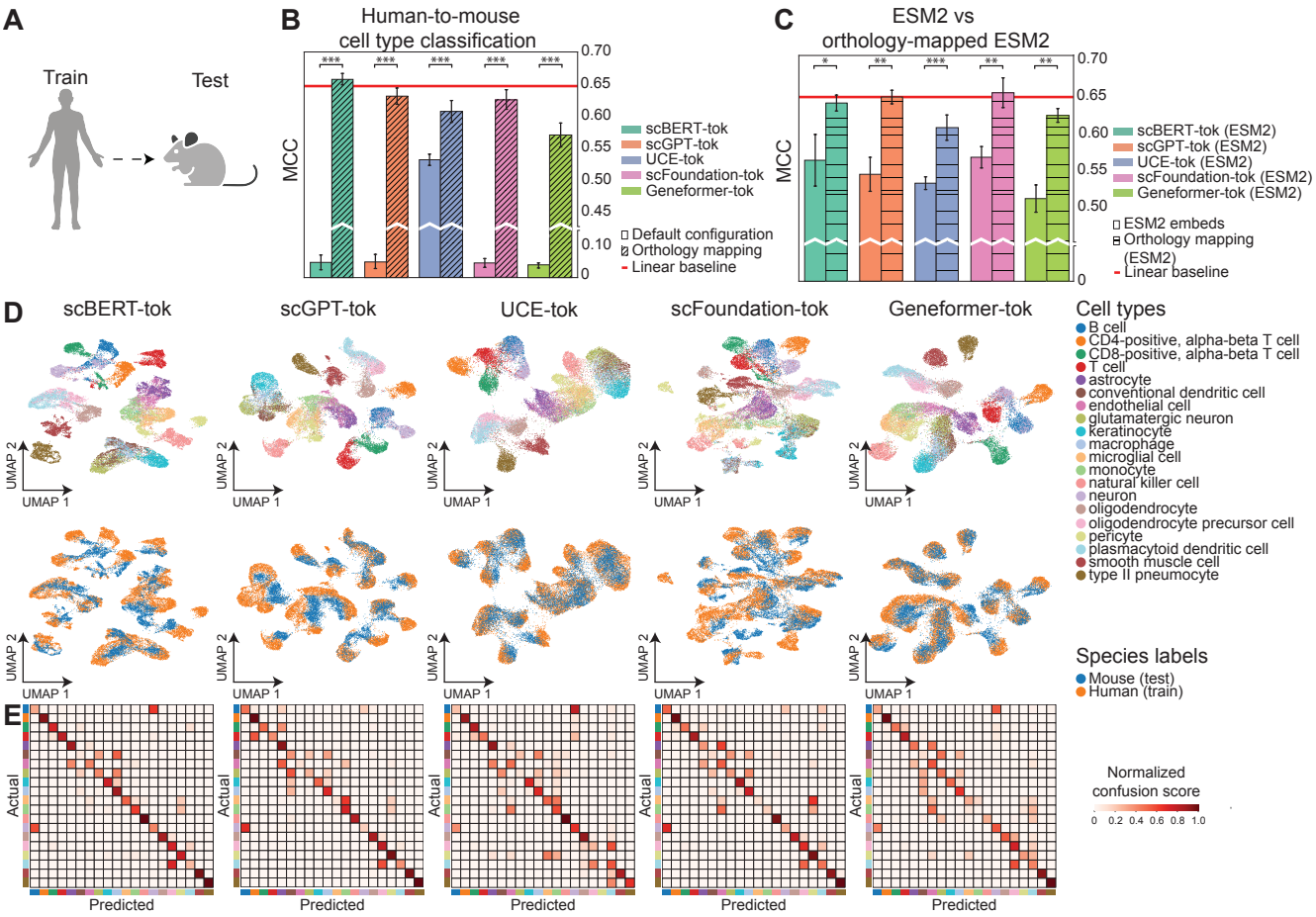

Figure 3: Evaluating the cross-species generalization capacity of scFMs. A. Schematic of the cross-species evaluation: models are trained on human cells and evaluated on mouse cells from matched cell types. **B.** Performance on the mouse test set for five scFM tokenizers, shown for each model's default tokenization (solid) and after orthology-based human $\rightarrow$ mouse gene mapping (diagonal hatch). Bars show MCC across seeds (error bars: s.d., $n = 5$ random seeds); Significance was assessed using paired t-tests with Holm correction ($p < 0.05$, $p < 0.01$, $p < 0.001$). A red horizontal line marks the linear baseline. **C.** Ablations of the gene identity module ($F_{\mathbf{G}}$): replacing each model's $F_{\mathbf{G}}$ with ESM2 embeddings (solid) or with ESM2 embeddings after orthology remapping (horizontal hatch). A red horizontal line marks the linear baseline. **D.** UMAP visualizations of the best-performing run for each tokenizer, colored by cell type (top) and species (bottom). **E.** Confusion matrices showing per-cell type precision and recall under cross-species transfer.

inherit a species-specific gene vocabulary, making cross-species evaluation a stringent benchmark of tokenizer generalization. To test this, we trained models for each tokenizer on human cells and evaluated them on mouse cells without additional finetuning, using what we refer to as the `cross-species` dataset (**Fig.** 3A).

We evaluate two strategies for producing species-comparable cell representations. (1) *Sequence-based gene identity*: UCE-tok's $F_{\mathbf{G}}$ represents each protein-coding gene as an ESM2 embedding of its protein sequence, yielding inherently species-agnostic representations. (2) *Orthology-based mapping*: for tokenizers lacking a sequence-based $F_{\mathbf{G}}$, mouse genes are mapped to their human orthologs prior to tokenization, aligning token identities with the human vocabulary used during training [29].

We first evaluated each tokenizer using its native configuration. scFoundation-tok, scGPT-tok, and

Geneformer-tok all use randomly initialized embeddings for $F_{\mathbf{G}}$. scBERT-tok uses Gene2vec embeddings pretrained on human genes, with mouse-specific (out-of-vocabulary) genes represented by random vectors. In this no-mapping setting, only UCE-tok achieved informative cross-species performance, due to its sequence-derived $F_{\mathbf{G}}$ (**Fig.** 3B).

We next compared tokenizer performance while preserving each method's $F_{\mathbf{G}}$, $F_{\mathbf{E}}$, and $F_{\mathbf{C}}$ modules under orthology-based mapping, which improved performance for all models (**Fig.** 3B). scBERT-tok performed best (0.66), followed by scGPT-tok (0.63), scFoundation-tok (0.63), UCE-tok (0.61), and Geneformer-tok (0.57). Notably, UCE-tok benefited from orthology mapping, even though it implicitly encodes orthologs. A linear baseline using the same orthology mapping performed similarly to the top-performing tokenizer scBERT-tok.

To directly test a species-agnostic $F_{\mathbf{G}}$, we performed an ablation in which each tokenizer's original $F_{\mathbf{G}}$ was replaced with ESM2 embeddings, while $F_{\mathbf{E}}$ and $F_{\mathbf{C}}$ were left unchanged (UCE-tok already uses ESM2 and was not ablated). Under this shared setting, scFoundation-tok, scGPT-tok, scBERT-tok, and Geneformer-tok all outperformed UCE-tok (**Fig.** 3C), indicating that UCE's cross-species advantage stems mostly from its sequence-derived $F_{\mathbf{G}}$, not from its $F_{\mathbf{E}}$ or $F_{\mathbf{C}}$.

Motivated by the gains from orthology mapping, we applied the same mapping to the ESM2 variants of each tokenizer. Across models, ESM2+orthology outperformed ESM2-only (**Fig.** 3C), consistent with improved alignment to the human training vocabulary and reduced out-of-vocabulary shift. Practically, orthology mapping and species-agnostic $F_{\mathbf{G}}$ are complementary: orthology mapping is advantageous where high-confidence maps exist, while a sequence-based $F_{\mathbf{G}}$ (e.g., UCE/ESM2) provides a robust, biologically grounded alternative when mappings are incomplete or uncertain.

UMAP visualizations of default scFM tokenizers under orthology mapping provide a qualitative view of each tokenizer's embedding space, with cells colored by type and species (**Fig.** 3D). Cells of the same type within each species cluster tightly, and matched human-mouse cell types partially integrate in the embedding space. These qualitative patterns are reflected quantitatively in the confusion matrices (**Fig.** 3E).

Overall, UCE-tok emerged as the strongest mapping-free tokenizer for cross-species generalization, owing to its sequence-based $F_{\mathbf{G}}$ that confers species-comparable gene identities. When $F_{\mathbf{G}}$ is standardized (ESM2 across models) or orthology mapping is applied, tokenizers with stronger $F_{\mathbf{E}}$ and $F_{\mathbf{C}}$ components can surpass its performance. Nevertheless, for poorly annotated or non-model species lacking reliable orthology mappings, UCE-tok's ESM2-based $F_{\mathbf{G}}$ remains the most practical and robust choice.

Evaluating scFM generalization to spatial transcriptomics

Unlike scRNA-seq data, which typically measures most genes in the transcriptome, many imaging-based spatially-resolved transcriptomics (SRT) datasets measure only a small panel of genes (often fewer than 1,000), and cross-study gene panels are often disjoint or only partially overlapping [30, 31]. This panel mismatch creates a natural testbed for gene generalization, as datasets often share only a limited subset of genes (**Fig.** 4A).

To first establish a within-dataset control before testing cross-panel generalization, we evaluated cell

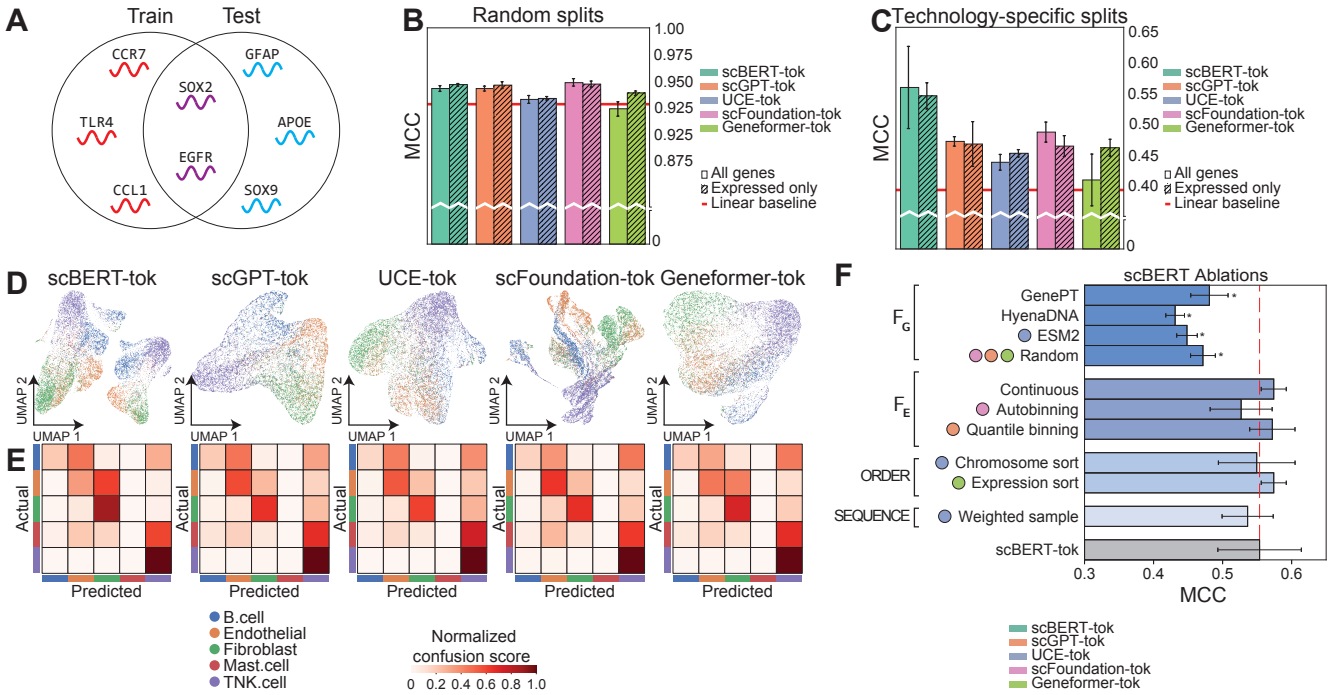

Figure 4: Spatial transcriptomics gene-panel generalization. A. Schematic of the gene-panel generalization task. **B.** Bar plots comparing tokenization strategies on random IID splits, reporting MCC for all genes and expressed-only genes. **C.** Bar plots comparing the same strategies under the `overlap-35` setting (35 shared genes). **D.** UMAP visualizations of the best-performing run for each scFM tokenizer. **E.** Confusion matrices for each tokenizer. **F.** Ablation of the best-performing tokenizer, scBERT-tok, across HEIMDALL modules. Significance was assessed using paired tests with Holm correction ($p < 0.05$, $p < 0.01$, $p < 0.001$). *Note:* In panels B-C, error bars show s.d. across 5 random seeds ($n = 5$); in panel F, error bars show s.d. across 6 random seeds ($n = 6$).

type classification on three ovarian cancer SRT samples with distinct gene panels [32] under independent and identically distributed (IID) splits, where training and test cells were drawn from the same distribution. Performance was uniformly high with minimal inter-model variance (**Fig.** 4B), indicating that tokenizer choice has little impact in IID settings.

We next evaluated performance under gene-panel shift using two non-IID benchmarks derived from three datasets: `overlap-35` (train panel 140 genes → test panel 280 genes; 35 shared) and `overlap-113` (train 280 genes → test 1,000 genes; 113 shared). On `overlap-35`, scBERT-tok performed best (0.55), followed by scGPT-tok, scFoundation-tok, and Geneformer-tok (0.47), with UCE-tok lowest (0.46) (**Fig.** 4C). All models exceeded a linear baseline (0.40), indicating that structured representations capture information beyond raw counts. UMAP visualizations and confusion matrices corroborated these rankings (**Fig.** 4D-E).

To account for tokenizer differences in handling non-expressed genes (see **Methods**), we evaluated both *expressed-only* and *all-genes* settings. This had little effect except for Geneformer-tok, which improved from 0.40 to 0.47 when restricted to expressed genes – consistent with its expression-ranking ORDER being sensitive to many zeros in the input (**Fig.** 4C).

We next used HEIMDALL 's modularization to identify the source of scBERT-tok's advantage. Because REDUCE is shared across tokenizers, we ablated only the remaining modules – $F_{\mathbf{G}}$, $F_{\mathbf{E}}$, and the

$F_{\mathbf{C}}$ submodules ORDER and SEQUENCE (**Fig.** 3F). $F_{\mathbf{G}}$ had the largest impact: Gene2vec remained strongest, with significant gains over GenePT, ESM2, and random (Holm-adjusted $p < 0.05$; paired tests across seeds). To probe this advantage, we analyzed the representational properties of each $F_{\mathbf{G}}$ (**Fig.** S3). Although Gene2vec embeddings showed weaker clustering of Gene Ontology terms than ESM2 or GenePT, co-expressed genes in the `overlap-35` benchmark had higher similarity in its embedding space (**Fig.** S3B-C). This pattern aligns with scBERT-tok's performance margin, suggesting that co-expression priors stabilize representations for genes appearing only in the test set. Results on `overlap-113` mirrored these trends, with scBERT-tok leading and UCE-tok trailing (**Fig.** S2). Changing $F_{\mathbf{E}}$ yielded smaller but consistent gains – particularly continuous embeddings and quantile binning outperformed other $F_{\mathbf{E}}$ variants. Modifications to ORDER, particularly the shift from random ordering to expression-based ordering, also led to small gains – while modifying SEQUENCE had minimal effect.

Together, these results show that under gene-panel shift, tokenizer design – particularly $F_{\mathbf{G}}$, with smaller gains from $F_{\mathbf{E}}$ and ORDER– dominates performance. scBERT-tok consistently performs highest, UCE-tok lowest, and other tokenizers fall in between. These differences emerge only under generalization, not IID settings, indicating that a co-expression informed $F_{\mathbf{G}}$ and a well-designed $F_{\mathbf{E}}$ and ORDER are critical for scFMs intended to generalize across gene panels.

Single-cell perturbation inference via reverse perturbation

We next evaluated scFM tokenization strategies on the task of *reverse perturbation prediction*, which inverts the standard perturbation prediction formulation [4]. Instead of predicting a cell's response to a given perturbation, the model is provided a target expression state and must identify perturbations likely to induce it. This formulation directly links cellular states to potential interventions, making it highly relevant for hypothesis generation and therapeutic target discovery.

We benchmarked tokenizers on the Norman single- and double-gene knockout dataset [33], which we processed into the `reverse-perturbation` dataset, framing the task as paired-cell classification where each instance consists of a control and its corresponding perturbed cell (**Fig.** 5A; task construction described in **Methods**). For paired-cell tasks, HEIMDALL introduces an AGGREGATOR module, which merges the individual embeddings of two cells provided by the transformer component into a single representation. For this task, we chose the asymmetric concatenation implementation of the AGGREGATOR module (see **Methods**). All models were benchmarked under matched conditions as in prior sections.

Performance varied substantially across tokenizers: scBERT-tok performed highest with a mean MCC of 0.39, followed by Geneformer-tok (0.38), scGPT-tok (0.31), scFoundation-tok (0.30), and UCE-tok (0.17) in order (**Fig.** 5B). We further quantified accuracy using hit-rate at threshold k, where $k = 1$ tests if the correct perturbation ranks first and larger k measure inclusion within the top-k predictions (**Fig.** 5C). All tokenizers showed a sharp increase in accuracy from $k = 1$ to $k = 10$, followed by smaller gains up to $k = 20$. Rankings were stable through $k \leq 15$ (scBERT-tok highest, UCE-tok lowest), with scFoundation-tok slightly surpassing Geneformer-tok at $k = 20$.

Next, we evaluated whether each model's predictions preserved gene-level semantics by comparing each model's top-1 predicted knockout to the gene ontology (GO) family of the true gene [34] using

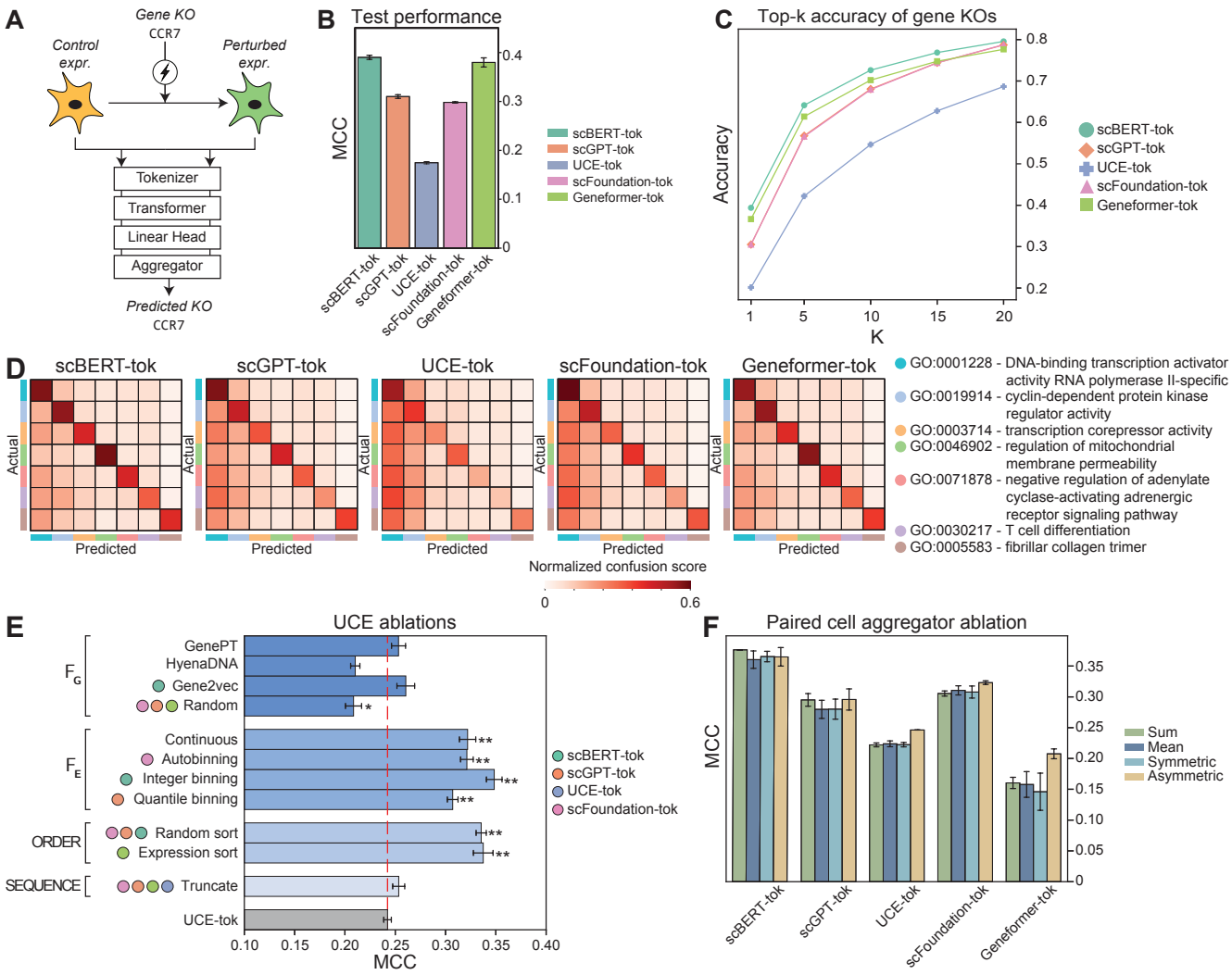

Figure 5: Comparison of performance on reverse perturbation prediction via HEIMDALL. A. Schematic of the reverse perturbation task, where perturbations are predicted from paired cells (control-perturbed pairs for single knockouts, or double knockouts where the first perturbation serves as the reference). **B.** Bar plots comparing cell tokenization strategies across scBERT, scGPT, UCE, scFoundation, and Geneformer, showing mean MCC $\pm$ s.d. across runs. **C.** Hit-rate (accuracy) of each method across k-thresholds. **D.** Gene-family heatmaps comparing predicted versus true knockout family memberships. **E.** HEIMDALL ablations of UCE-tok for each cell identity module. Significance was assessed using paired tests with Holm correction ($p < 0.05$, $p < 0.01$, $p < 0.001$). **F.** Ablation of paired-cell AGGREGATOR strategies across five scFMs. *Note:* Error bars show s.d. across $n = 3$ random seeds.

row-normalized confusion matrices (**Fig.** 5D). scBERT-tok and Geneformer-tok showed the strongest concentration on the diagonal and fewest cross-family errors, suggesting that incorrect predictions often fall within the correct functional family. In contrast, scGPT-tok and scFoundation-tok distributed probability mass across adjacent families, while UCE-tok exhibited the most diffuse off-diagonal signal and biased predictions toward most prevalent families.

Using HEIMDALL's per-module ablation, we examined why UCE-tok underperforms in reverse perturbation prediction (**Fig.** 5E). Modules lacking explicit expression information (F_{G} and SEQUENCE) had minor effects: within F_{G}, ESM2 only exceeded random embeddings with significance (Holm-adjusted

$p < 0.05$), while swaps to GenePT and Gene2vec did not. The largest improvements came from adding expression-aware modules ($F_{\mathbf{E}}$ and ORDER), which follows naturally from UCE-tok's default omission of expression encodings. In $F_{\mathbf{E}}$, continuous, autobinning, integer binning, and quantile binning each surpassed the UCE default (all Holm-adjusted $p < 0.01$), with integer binning ($F_{\mathbf{E}}$ from scBERT-tok) strongest (MCC of 0.35 versus 0.25). Further significant improvements came from replacing UCE-tok's chromosome-based ORDER with alternatives that better reflect expression (Geneformer-tok's expression ordering) or by relaxing ordering assumptions with random ordering (Holm-adjusted $p < 0.01$). These results align with the original UCE study, which reported that adding chromosomal metadata led to a modest decrease in performance [10]. Finally, we performed an ablation of the paired-cell AGGREGATOR module, comparing (1) elementwise mean, (2) elementwise sum, (3) symmetric concatenation, and (4) asymmetric concatenation (see **Methods**). For each tokenizer, asymmetric concatenation achieved either exceeded or matched the performance of other implementations, supporting its use in the main analyses (**Fig.** 5F).

Overall, rigorous evaluation with HEIMDALL reveals that changes to the $F_{\mathbf{E}}$ and ORDER tokenization modules has the most impact on performance on the reverse perturbation task. For UCE-tok, which lacks expression encodings by default, including *any* $F_{\mathbf{E}}$ substantially improved performance. Combining scBERT-tok's $F_{\mathbf{E}}$ and Geneformer-tok's ORDER yields the largest boost – highlighting these modules as key factors underlying top-model performance.

Discussion

Despite rapid progress in scFM performance, the effect of individual tokenization choices remains poorly understood. HEIMDALL addresses this gap by decomposing tokenizers into modules for gene identity ($F_{\mathbf{G}}$), expression encoding ($F_{\mathbf{E}}$), and cell construction ($F_{\mathbf{C}}$), and by standardizing evaluation. Through faithful reimplementations within a unified framework, HEIMDALL turns monolithic tokenizers into interchangeable, analyzable modules, enabling controlled and interpretable ablations that support principled development.

Empirically, HEIMDALL shows that performance is driven primarily by pretrained $F_{\mathbf{G}}$ and expression encoding choices – explicitly via $F_{\mathbf{E}}$, implicitly via ORDER– with hybrid designs outperforming existing scFMs. These findings provide actionable guidance: rather than relying on a single tokenizer, one can recombine $F_{\mathbf{G}}$, $F_{\mathbf{E}}$, and $F_{\mathbf{C}}$ modules, quantify each module's contributions, and iterate within a common benchmarking scaffold. In doing so, HEIMDALL enables cumulative comparisons across downstream tasks and clarifies which inductive biases matter most – $F_{\mathbf{G}}$ priors (protein-sequence versus co-expression), $F_{\mathbf{E}}$ encodings (bin versus continuous), ORDER choices (expression ranking versus chromosome ordering), and sparsity handling – among others.

This study has several limitations. First, our pretraining ablation used only an MLM objective; expanding to other objectives and larger corpora – both feasible in HEIMDALL– may refine conclusions about module importance. Second, we evaluated a small, fixed transformer; scaling or exploring alternative architectures (for example, state-space models) could shift tokenizer trade-offs. Finally, while

we focused on cell-type classification and reverse perturbation, extending to perturbation-response modeling, batch integration, gene regulatory network inference, and spatial tasks will further probe when particular tokenization choices succeed.

HEIMDALL is designed to support such extensions. New pretraining objectives, corpora, architectures, and tasks can be added as plug-ins with minimal engineering. Beyond the $F_{\mathbf{G}}$ variants evaluated here (for example, GenePT and HyenaDNA), future work can integrate multimodal priors – chromatin accessibility, histone modifications, and sequence context – across $F_{\mathbf{G}}$, $F_{\mathbf{E}}$, and $F_{\mathbf{C}}$, and extend to multicellular representations for cell-cell communication and spatial organization. Looking ahead to *virtual cells* [26], unified tokenization of transcriptomic, genomic, epigenomic, and proteomic signals will be essential. Our use of HyenaDNA as an $F_{\mathbf{G}}$ illustrates one route to sequence-aware tokenization; deeper integration of regulatory and epigenomic signals may enable the robust representations needed for virtual-cell reasoning.

In summary, HEIMDALL provides a rigorous, modular framework for systematically evaluating, ablating, and improving cell tokenization within scFMs. By isolating module-level effects, enforcing standardized and cumulative benchmarking, and enabling rapid testing of new tokenizer components – including faithful reimplementations under a unified API – HEIMDALL is poised to accelerate the development of more capable, generalizable, and ultimately multimodal single-cell foundation models.

Methods

Tokenization paradigm for single-cell foundation models

To enable measured comparison and benchmarking of single-cell foundation models (scFMs), HEIMDALL represents their breadth and scope within a common functional paradigm. Using HEIMDALL, we reformulate several recently proposed scFMs under a unified, compositional framework.

For an input transcriptomic dataset $Y \in \mathbb{R}_+^{N \times G}$ with gene features drawn from the set of all genes $\mathcal{G}_{all}$ and for a sequence embedding model with maximum sequence length L and hidden dimension K, the scFM function is defined as:

$$f_{scFM}(\mathcal{G}, y_i) := (f_\theta \circ f_{\text{tokenizer}})(\mathcal{G}, y_i), \tag{1}$$

where $f_{\text{tokenizer}}$ is the "cell tokenizer" that converts a cell's gene expression vector $y_i \in \mathbb{R}^G$ and gene set $\mathcal{G} = \{g_0, \ldots, g_{G-1}\} \in \binom{\mathcal{G}_{all}}{G}$ into an $L \times K$-dimensional real-valued tokenization, and $f_\theta : \mathbb{R}^{L \times K} \to \mathbb{R}^K$ applies the transformer-based encoder to the tokenizer output. Here, θ are the encoder's learnable parameters. The tokenizer is further decomposed as:

$$f_{\text{tokenizer}}(\mathcal{G}, y_i) := F_C(F_G(\mathcal{G}), F_E(y_i)), \tag{2}$$

where $F_G : \binom{\mathcal{G}_{all}}{G} \to \mathbb{R}^{G \times K}$ tokenizes gene identities, $F_E : \mathbb{R}_+^G \to \mathbb{R}^{G \times K}$ tokenizes gene expressions, and $F_C : \mathbb{R}^{G \times K} \times \mathbb{R}^{G \times K} \to \mathbb{R}^{L \times K}$ combines the outputs of the F_G and F_E.

To capture the breadth of pretraining tasks and downstream applications, we model task-specific decoders ("heads") $f_\phi : \mathbb{R}^K \to \mathcal{L}$, which map the scFM output to a label space $\mathcal{L}$. For example, for cell-type annotation over C cell types, the label space consists of one-hot C-dimensional vectors (i.e., $\mathcal{L} = \{0, 1\}^C$); for gene expression reconstruction, $\mathcal{L} = \mathbb{R}_+^G$.

Fig. S1 illustrates the HEIMDALL framework.

Abstraction of gene identity-based encodings via $F_{\mathbf{G}}$

The $F_{\mathbf{G}}$ component converts gene names/identifiers into K-dimensional real-valued embedding vectors, which are then forwarded to $F_{\mathbf{C}}$.

- **Random initialization.** Each gene is assigned a randomly initialized embedding vector, ensuring unique embeddings per gene.
- **Pretrained.** Several methods derive pretrained gene embeddings from external priors:
  - **ESM2.** The amino acid sequence of each gene's protein product(s) is embedded with ESM2 [35]; multiple protein products are averaged.
  - **Gene2vec.** The Gene2vec [36] approach learns embeddings from gene coexpression patterns so co-expressed genes are nearby in embedding space.
  - **GenePT.** GenePT [6] uses the gene name and its NCBI text description as natural-language input to GPT-3.5 [37]; the output is taken as the embedding.

- **HyenaDNA.** This approach embeds the gene's DNA sequence (ENSEMBL release 112) with HyenaDNA [38]; the last token representation is used as the embedding.

If an embedding is unavailable for a given gene in a particular pretrained set, that gene is removed before subsequent tokenization steps. To resolve dimensionality mismatches between pretrained embeddings and the inherent dimensionality of the transformer model, we standardize and apply PCA to reduce all gene embeddings to 128 dimensions.

Abstraction of gene expression-based encodings via $F_{\mathbf{E}}$

The $F_{\mathbf{E}}$ component converts the expression values of a cell into a processed expression vector and a corresponding K-dimensional embedding vector; both are forwarded to $F_{\mathbf{C}}$.

- **No-op.** Outputs a constant zero vector per gene regardless of expression level (used by Geneformer and UCE).
- **Continuous.** A two-layer fully connected perceptron maps raw expression values to expression embeddings.
- **Quantile binning.** Expression values are assigned to B bins; each bin has a unique learnable embedding vector. Zero-valued expression is mapped to a dedicated "zero bin" (index 0). We use scGPT's default $B = 51$.
- **Integer binning.** Expression values are partitioned into B bins by rounding each gene y_{ig} down and clipping to $\min(\lfloor y_{ig} \rfloor, B - 1)$. We use scBERT's default $B = 7$ for all benchmarks.
- **Autobinning.** Raw expression values are input to a two-layer fully connected perceptron that outputs B weights over learnable "autobin" embeddings; the final expression embedding is their weighted sum. We use scFoundation's default $B = 100$ for all benchmarks.

HEIMDALL also allows the option of retaining or discarding zero-expression genes prior to $F_{\mathbf{E}}$, reflecting the scFM literature practices that include non-expressed genes in the input.

Abstraction of single-cell representation functions via the $F_{\mathbf{C}}$ module

The $F_{\mathbf{C}}$ module constructs the final tokenized single-cell representation by composing the outputs of $F_{\mathbf{G}}$ and $F_{\mathbf{E}}$. We partition $F_{\mathbf{C}}$ into three sequentially submodules:

1. The ORDER function. Determines an intrinsic ordering of genes in the input cell, which SEQUENCE can use to place gene tokens into a meaningful sequence.
    - **Expression sorting.** Genes are ordered by their expression within the cell; expression values are normalized by the gene's median across all cells prior to sorting (as in Geneformer).
    - **Chromosome sorting.** Genes are ordered by genomic coordinates in a two-stage process. First, genes are grouped into "chromosome blocks" by chromosome-of-origin; each block is delimited by start/end tokens, with start tokens unique to each chromosome and species. Because chromosomes have no intrinsic order, blocks are randomly permuted per cell. Second,

within each block, genes are ordered by genomic start position. The permuted blocks are then concatenated to form the final sequence.

- **Random ordering.** Genes receive a random permutation per cell.

2. The SEQUENCE function. This module constructs the sequence of tokens input to the final transformer architecture. It can use the gene order output by the ORDER module to sequence genes. Beyond handling gene tokens, SEQUENCE may also inject metadata-based tokens to incorporate information complementary to the transcriptomic modality. For all SEQUENCE implementations, if the number of tokens exceeds the context length L, truncate to L; otherwise append `[PAD]` tokens to reach L.

   - **Truncation.** Place gene tokens according to ORDER and truncate to context length L.
   - **Weighted sampling.** Sample genes with replacement, with probabilities proportional to their expression within the cell, until reaching L.

3. The REDUCE function. This module dictates how the $F_{\mathbf{G}}$ and $F_{\mathbf{E}}$ are combined for each gene token.

   - **Identity.** The $F_{\mathbf{G}}$ identity embeddings are directly used as the combined embeddings, and the $F_{\mathbf{E}}$ expression embeddings are ignored.
   - **Sum.** The $F_{\mathbf{G}}$ identity embeddings and $F_{\mathbf{E}}$ expression embeddings are summed element-wise to produce the combined embeddings.

Together, $F_{\mathbf{G}}$, $F_{\mathbf{E}}$ and $F_{\mathbf{C}}$ yield the overall tokenization scheme (tokenizer) for an scFM, applied individually to each cell in an scRNA-seq dataset.

Model architectures for processing tokenizer outputs

To process and extract information from a single-cell tokenization, scFMs use several machine learning model architectures. Most scFMs adopt a standard transformer architecture [39, 40], with stacked multi-head attention layers applied to the gene-token sequence. HEIMDALL includes the following options:

- **Transformer.** The gene token sequence for each cell is input to a transformer with n_{layer} encoder blocks. Each block consists of a multi-head attention block followed by a fully connected multi-layer perceptron.
- **Weighted token average.** For each cell, the weighted average of the K-dimensional token embeddings is used as the final embedding, with weights proportional to raw gene expression (as in GenePT [6] and CellPLM [41]).
- **Linear baseline.** The raw expression vector is fed directly to a single-layer fully-connected linear encoder to produce a K-dimensional cell embedding.

Formulation of tasks

HEIMDALL flexibly supports the definition, configuration, and evaluation of diverse downstream tasks for scFMs. Defining a task requires specifying labels, a task-specific decoder ("head") architecture, and a loss function (**Fig.** S1). Although not explored in this work, as a natural consequence of this abstraction, HEIMDALL natively supports multi-task learning.

Classification tasks

For classification tasks, precomputed class labels are provided for the input single-cell data, and the model predicts these labels for each cell. Examples include cell-type annotation (multiclass) and disease-risk prediction (binary).

- **Cell-type annotation.** A multi-class classification task in which the model predicts the cell type using the embedding of the `[CLS]` token. The loss is cross-entropy.

Regression tasks

For regression tasks, each cell is paired with one or more continuous targets (e.g., gene perturbation effect sizes, pseudotime, or per-gene expression), and the model predicts these values from the tokenized input. We formulate this as single- or multi-output regression and optimize mean squared error (MSE). Example applications include (i) perturbation prediction – estimating continuous gene knockout effects – and (ii) pretraining via expression reconstruction, where the model predicts gene expression and is trained with an MSE objective.

Pretraining tasks

Our framework supports pretraining tasks to train HEIMDALL on large datasets in a self-supervised manner. For such tasks, labels are generated during training by the dataset implementation within HEIMDALL. Examples include:

- **Expression reconstruction.** Reconstruct the input gene expression vector $y_i \in \mathbb{R}^G$ for each cell i (a regression task).
- **Masked language modeling.** As in NLP [42], masked language modeling (MLM) entails masking a random proportion of gene tokens in the cell sentence and replace them with `[MASK]` tokens. The model then predicts the identities of the masked tokens (a multiclass task).

Definition of paired-input tasks

Besides single-input tasks, HEIMDALL supports paired-input tasks in which each sample consists of a pair of cells. Each cell is passed through the model, and the resulting embeddings are reduced to a "pair embedding" using one of:

- **Mean.** Element-wise average.

- **Sum.** Element-wise sum.
- **Symmetric concatenation.** Concatenate embeddings and pass through a single-layer full connected perceptron to yield a K-dimensional output; repeat with the reverse order, then sum the two outputs to produce the pair embedding.
- **Asymmetric concatenation.** Concatenate embeddings in a fixed order and pass through a single-layer full-connected perceptron to yield a K-dimensional, order-sensitive output (no reserve-order pass).

Extending HEIMDALL via novel implementations of tokenizer modules

Beyond reproducing existing scFM tokenizers, HEIMDALL provides standardized, well-documented interfaces for $F_{\mathbf{G}}$, $F_{\mathbf{E}}$, ORDER, SEQUENCE, and REDUCE, enabling plug-and-play development of novel tokenization modules. We illustrate this extensibility by implementing and evaluating new modules for $F_{\mathbf{G}}$, $F_{\mathbf{E}}$, and REDUCE. First, we add a HyenaDNA-based $F_{\mathbf{G}}$ that provides sequence-derived gene-identity embeddings and include it in ablations throughout the paper. Second, we co-opt GenePT's use of ChatGPT embeddings for NCBI text descriptions of genes as a novel $F_{\mathbf{G}}$– note that this contrasts from the original GenePT paper, which simply averages these gene tokens as opposed to using a transformer. Third, we introduce a continuous $F_{\mathbf{E}}$ that maps raw expression values to embeddings via a two-layer multilayer perceptron (MLP). While all five HEIMDALL-reproduced scFM tokenizers default to a sum REDUCE, tokenizers that omit explicit expression encodings in $F_{\mathbf{E}}$ (e.g., UCE and Geneformer) can also operate with an identity REDUCE. Comprehensive API documentation and examples are available in the HEIMDALL GitHub repository.

Code Availability

HEIMDALL is released as an open-source Python package on the Python Package Index (`pip install sc-heimdall`). Furthermore, HEIMDALL is a fully open-source project hosted on GitHub:

https://github.com/ma-compbio/Heimdall

The GitHub repository includes reference implementations of the cell tokenizer components ($F_{\mathbf{G}}$, $F_{\mathbf{E}}$, ORDER, SEQUENCE, REDUCE), model architectures, training/evaluation scripts, and the exact Hydra configuration files used in this study.

Data Availability

- The `sc-tab` dataset [27] is publicly available for download at: https://github.com/theislab/scTab.
- The `overlap-113` and `overlap-35` [32] datasets are publicly available for download at: https://zenodo.org/records/12613839.
- The `cross-species` dataset was processed from CELLxGENE [12].
- The `reverse perturbation` [33] dataset is publicly available for download at: https://www.ncbi.nlm.nih.gov/geo/query/acc.cgi?acc=GSE133344.

A detailed description of how to download and construct these datasets can be found in the **Supplemental Information**.

Acknowledgements

The authors would like to thank Yang Zhang, Junjie Tang, Wenduo Cheng, Shike Wang, Gün Kaynar and Xue Er Ding for helpful discussions and for assistance with dataset construction and curation. This work was supported, in part, by National Institutes of Health Common Fund 4D Nucleome Program grant UM1HG011593 (J.M.); National Institutes of Health Common Fund Cellular Senescence Network Program grant UH3CA268202 (J.M.); and National Institutes of Health grants R01HG007352 (J.M.), R01HG012303 (J.M.), R21DA061481 (J.M.), and R03OD039980 (J.M.). J.M. was additionally supported by the Ray and Stephanie Lane Professorship, a Guggenheim Fellowship from the John Simon Guggenheim Memorial Foundation, a Google Research Award, and a Single-Cell Biology Data Insights award from the Chan Zuckerberg Initiative. S.A. was supported by the NIH Training Grant T32EB009403 (2023-2024). N.H. was supported by a National Science Foundation Graduate Research Fellowship. S.K. and S.L. are Lane Fellows. The funders had no role in study design, data collection and analysis, decision to publish or preparation of the manuscript.

Author Contributions

Conceptualization: E.H., S.A., N.H., S.K., and J.M.; Methodology: E.H., S.A., N.H., and S.K.; Software: E.H., S.A., N.H., and S.K.; Investigation: E.H., S.A., N.H., R.L., E.T., S.L., M.Y., S.K., and J.M.; Writing: E.H., S.A., N.H., S.K., and J.M.; Funding Acquisition: J.M.

Competing Interests

The authors declare no competing interests.

References

[1] Jumper, J. *et al.* Highly accurate protein structure prediction with alphafold. *Nature* **596**, 583–589 (2021).

[2] Dalla-Torre, H. *et al.* Nucleotide transformer: building and evaluating robust foundation models for human genomics. *Nature Methods* 1–11 (2024).

[3] Moor, M. *et al.* Foundation models for generalist medical artificial intelligence. *Nature* **616**, 259–265 (2023).

[4] Cui, H. *et al.* scGPT: toward building a foundation model for single-cell multi-omics using generative AI. *Nature Methods* **21**, 1470–1480 (2024).

[5] Theodoris, C. V. *et al.* Transfer learning enables predictions in network biology. *Nature* **618**, 616–624 (2023).

[6] Chen, Y. & Zou, J. Simple and effective embedding model for single-cell biology built from chatgpt. *Nature Biomedical Engineering* **9**, 483–493 (2025).

[7] Levine, D. *et al.* Cell2sentence: teaching large language models the language of biology. *bioRxiv* 2023–09 (2024).

[8] Hao, M. *et al.* Large-scale foundation model on single-cell transcriptomics. *Nature Methods* **21**, 1481–1491 (2024).

[9] Yang, F. *et al.* scBERT as a large-scale pretrained deep language model for cell type annotation of single-cell rna-seq data. *Nature Machine Intelligence* **4**, 852–866 (2022).

[10] Rosen, Y. *et al.* Universal cell embeddings: A foundation model for cell biology. *bioRxiv* 2023–11 (2023).

[11] Tarhan, L. *et al.* Single Cell Portal: an interactive home for single-cell genomics data. *bioRxiv* (2023).

[12] Program, C. C. S. *et al.* CZ CELLxGENE Discover: a single-cell data platform for scalable exploration, analysis and modeling of aggregated data. *Nucleic Acids Research* **53**, D886–D900 (2025).

[13] Regev, A. *et al.* The human cell atlas. *eLife* **6**, e27041 (2017).

[14] Liu, T., Li, K., Wang, Y., Li, H. & Zhao, H. Evaluating the utilities of foundation models in single-cell data analysis. *bioRxiv* 2023–09 (2023).

[15] Lotfollahi, M. Toward learning a foundational representation of cells and genes. *Nature Methods* **21**, 1416–1417 (2024).

[16] Kedzierska, K. Z., Crawford, L., Amini, A. P. & Lu, A. X. Zero-shot evaluation reveals limitations of single-cell foundation models. *Genome Biology* **26**, 101 (2025).

[17] Ahlmann-Eltze, C., Huber, W. & Anders, S. Deep-learning-based gene perturbation effect prediction does not yet outperform simple linear baselines. *Nature Methods* **22**, 1657–1661 (2025).

[18] Boiarsky, R. *et al.* Deeper evaluation of a single-cell foundation model. *Nature Machine Intelligence* **6**, 1443–1446 (2024).

[19] Bendidi, I. *et al.* Benchmarking transcriptomics foundation models for perturbation analysis : one PCA still rules them all. *arXiv* (2024).

[20] Li, C. *et al.* Benchmarking ai models for in silico gene perturbation of cells. *bioRxiv* 2024–12

(2024).

[21] DenAdel, A. *et al.* Evaluating the role of pre-training dataset size and diversity on single-cell foundation model performance. *bioRxiv* 2024.12.13.628448 (2024).

[22] De Waele, G., Menschaert, G. & Waegeman, W. A systematic assessment of single-cell language model configurations. *bioRxiv* 2025–04 (2025).

[23] Richter, T., Bahrami, M., Xia, Y., Fischer, D. S. & Theis, F. J. Delineating the effective use of self-supervised learning in single-cell genomics. *Nature Machine Intelligence* **7**, 68–78 (2025).

[24] Ahia, O. *et al.* Do all languages cost the same? tokenization in the era of commercial language models. *arXiv* (2023).

[25] Sennrich, R., Haddow, B. & Birch, A. Neural machine translation of rare words with subword units. *arXiv* (2015).

[26] Bunne, C. *et al.* How to build the virtual cell with artificial intelligence: Priorities and opportunities. *Cell* **187**, 7045–7063 (2024).

[27] Fischer, F. *et al.* scTab: Scaling cross-tissue single-cell annotation models. *Nature Communications* **15**, 6611 (2024).

[28] Breschi, A., Gingeras, T. R. & Guigó, R. Comparative transcriptomics in human and mouse. *Nature Reviews Genetics* **18**, 425–440 (2017).

[29] stefanpeidli/mousipy: Translates an AnnData object with mouse gene symbols into one with human gene symbols by mapping orthologs from biomart. URL https://github.com/stefanpeidli/mousipy.

[30] Hu, Y. *et al.* Benchmarking clustering, alignment, and integration methods for spatial transcriptomics. *Genome Biology* **25**, 212 (2024).

[31] Haber, E., Deshpande, A., Ma, J. & Krieger, S. Unified integration of spatial transcriptomics across platforms. In *International Conference on Research in Computational Molecular Biology*, 371–375 (Springer, 2025).

[32] Yeh, C. Y. *et al.* Mapping spatial organization and genetic cell-state regulators to target immune evasion in ovarian cancer. *Nature Immunology* **25**, 1943–1958 (2024).

[33] Norman, T. M. *et al.* Exploring genetic interaction manifolds constructed from rich single-cell phenotypes. *Science* **365**, 786–793 (2019).

[34] Klopfenstein, D. *et al.* GOATOOLS: A python library for Gene Ontology analyses. *Scientific Reports* **8**, 1–17 (2018).

[35] Lin, Z. *et al.* Evolutionary-scale prediction of atomic-level protein structure with a language model. *Science* **379**, 1123–1130 (2023).

[36] Du, J. *et al.* Gene2vec: distributed representation of genes based on co-expression. *BMC Genomics* **20**, 82 (2019).

[37] Shen, H. *et al.* Generative pretraining from large-scale transcriptomes for single-cell deciphering. *iScience* **26** (2023).

[38] Nguyen, E. *et al.* Hyenadna: Long-range genomic sequence modeling at single nucleotide resolution. *Advances in Neural Information Processing Systems* **36**, 43177–43201 (2023).

[39] Vaswani, A. *et al.* Attention is all you need. *Advances in neural information processing systems* **30**

(2017).

[40] Szałata, A. *et al.* Transformers in single-cell omics: a review and new perspectives. *Nature Methods* **21**, 1430–1443 (2024).

[41] Wen, H. *et al.* CellPLM: Pre-training of cell language model beyond single cells. In *The Twelfth International Conference on Learning Representations* (2024).

[42] Devlin, J., Chang, M.-W., Lee, K. & Toutanova, K. BERT: Pre-training of deep bidirectional transformers for language understanding. In *Proceedings of the 2019 Conference of the North American Chapter of the Association for Computational Linguistics: Human Language Technologies (Vol. 1)*, 4171–4186 (2019).